

Dust storms modeling and their impacts on air quality and radiation budget over Iran using WRF-Chem

Khosro Ashrafi¹ · Majid Shafiepour Motlagh¹ · Soroush Esmacili Neyestani¹

Received: 12 April 2017 / Accepted: 30 June 2017 / Published online: 17 July 2017
© Springer Science+Business Media B.V. 2017

Abstract The main objective of this research work is to simulate dust storms and evaluate their impacts on air quality and radiation budget over Iran using WRF-Chem coupled model. Two appropriately strong dust storms: May 22–25, 2012 and April 22–25, 2015. According to the results, in the Middle East, countries where sources with highest emission rates are placed include Syria, Iraq, Saudi Arabia, Turkmenistan, and major hot spots inside Iran in the southwestern regions. During both of above storms, very high dust concentrations have been simulated. Domain and simulation period average dust concentration have been estimated to be 402 and 515 $\mu\text{g}/\text{m}^3$ over Iran during May-2012 and April-2015 dust storms, respectively. Also, 24 h average dust concentration exceeds 7000 $\mu\text{g}/\text{m}^3$ in some regions in the Middle East. Comparison of simulated and observed extinction coefficients and aerosol optical depths (AOD) shows an underestimation for domain averaged AOD. However, spatial and temporal distribution patterns of dust have been well simulated by the developed model. Using two parallel simulations with and without dusts, impacts of dust aerosols on radiation and some meteorological parameters have been evaluated. According to the results, dust aerosols led to negative short-wave (SW) radiative perturbation at the earth's surface and top of atmosphere (TOA). These radiative perturbations were positive for long-wave (LW) radiation. Stronger negative diurnal perturbations for sensible heat flux, rather than positive nocturnal perturbation which caused 24 h average perturbation to be negative. Nevertheless, the

weaker diurnal (negative) rather than nocturnal (positive) surface temperature perturbations made the 24-h average temperature perturbation positive.

Keywords Dust storms · Modeling · Aerosol · Air quality · Radiative perturbation · WRF-Chem

Introduction

Dust aerosols are produced mainly by wind erosion in arid and semi-arid regions around the world. Global dust emission is estimated to be about 3000 million tons annually (and a substantial amount of this emitted dust is deposited in the ocean). However, such estimates vary from 100 to 10,000 million tons in different studies (Shao 2008). The largest mineral dust emission sources in the world are located in the Sahara in the Middle East and central to Eastern Asian desert regions (Prospero et al. 2002). It is estimated that annual dust emission rates in these regions, which is also called dust belt, reach 1000–1300 million tons and attribute to more than three fourth of the global dust emissions (Ginoux et al. 2012).

Considering extended arid regions, the Middle East frequently experiences dust events. There are four major regions in the Middle East with most dust haze episodes. Sudan, Saudi Arabia, Iraq, Iran, Afghanistan, and Pakistan regularly experience dust storms. However, temporal and spatial distribution of dust events is not similar in different regions (Rezazadeh et al. 2013). Arid and semi-arid regions cover about 60% of Iran (approximately 1 million km^2). There are five regions over Iran where dust events frequently occur. These areas are Khuzestan Plain in southwestern Iran, coastal plain of the Persian Gulf, western part of Iran, Tabas region in the east central part of Iran, and Sistan region in southeast of Iran (Alizadeh-Choobari et al. 2015). Nevertheless, it is well

✉ Khosro Ashrafi
khashrafi@ut.ac.ir

¹ Department of Environmental Engineering, Faculty of Environment, University of Tehran, P.O. Box: 14155-6135, No. 15, Ghods Street, Enghelab ave, Tehran, Iran

accepted that a substantial amount of dust aerosols over Iran is emitted from transboundary sources, especially western neighbors such as Iraq and Syria (Shahsavani et al. 2012; Ashrafi et al. 2014).

Dust storms by injecting a substantial amount of dust particles into the atmosphere significantly affect the ambient air quality, climate, and human health in a wide range of ways. Particulate matters' concentration and consequently air quality index (AQI) might increase sharply during dust events and reach much higher values of the ambient air quality standards (Huang et al. 2013; Aryal et al. 2015). Several studies show that human exposure to high concentration of dust aerosols, especially fine particles, causes adverse health impacts such as cardiovascular disease, lung cancer, and premature mortality (Kakikawa et al. 2008; Giannadaki et al. 2014). Furthermore, interaction of dust and radiation has significant impacts on the Earth's energy balance. Dust aerosols directly affect the Earth's radiation budget by absorbing or scattering both short-wave (generally cooling effect) and long-wave (generally warming effect) radiation (Zhao et al. 2011; Choobari et al. 2014). On the other hand, the interaction between dust aerosols and clouds, which is called indirect effect, leads to modification in cloud's properties such as its microphysics and optical properties (Mahowald and Kiehl 2003; Sathesh and Krishna Moorthy 2005). Dust particles, also, have impacts on precipitation process by being used as cloud condensation or ice nuclei (DeMott et al. 2010; Kumar et al. 2011).

Several regional studies have been carried out on dust storm simulation and its impact on optical properties and radiation for different regions around the world. In one of such studies, dust transport from the Taklimakan Desert to Tibetan Plateau is simulated (Chen et al. 2013). The dust-induced radiative forcing is estimated to be -5.58 W/m^2 at the surface and -3.97 W/m^2 at top of the atmosphere over the Tibetan Plateau. Also, the results of modeling surface radiative forcing over the Gobi Desert and the North China Plain are estimated to be -21.1 and -13.1 W/m^2 , respectively, during a typical Asian dust storm (Liu et al. 2016). Kumar et al. (2014) evaluated the influences of a pre-monsoon dust storm on aerosol optical depth (AOD) and radiative perturbation over northern India. The average AOD value calculated in that study was about 0.68. Nevertheless, the observed MODIS average AOD indicates an underestimate in model results. Furthermore, a study on a winter-time dust event in the Arabian Peninsula estimates 18.4 Tg dust emission during the event (Kalenderski et al. 2013). The mean instantaneous radiative forcing over this region is estimated to be -14.1 W/m^2 . However, the maximum value reaches -205 W/m^2 over the Arabian Sea.

As mentioned above, dust storms and their impacts are simulated in many studies. However, very limited, if any, research focused on modeling the impacts of dust storms over Iran. Therefore, the main objective of this research work is to

numerically simulate emission sources, spatial and temporal distribution of dust aerosols, and the impacts of severe dust storms on optical properties and radiative perturbation over Iran. The paper is structured as follows: in “**Model and data**” section, the model (including settings and schemes) and observational data which have been used for this investigation are described. In “**Results and discussion**” section, the results of the simulation are discussed and compared with observations in five subsections. Finally, in the “**Conclusions**” section of this paper, the results and findings of this work have been concluded.

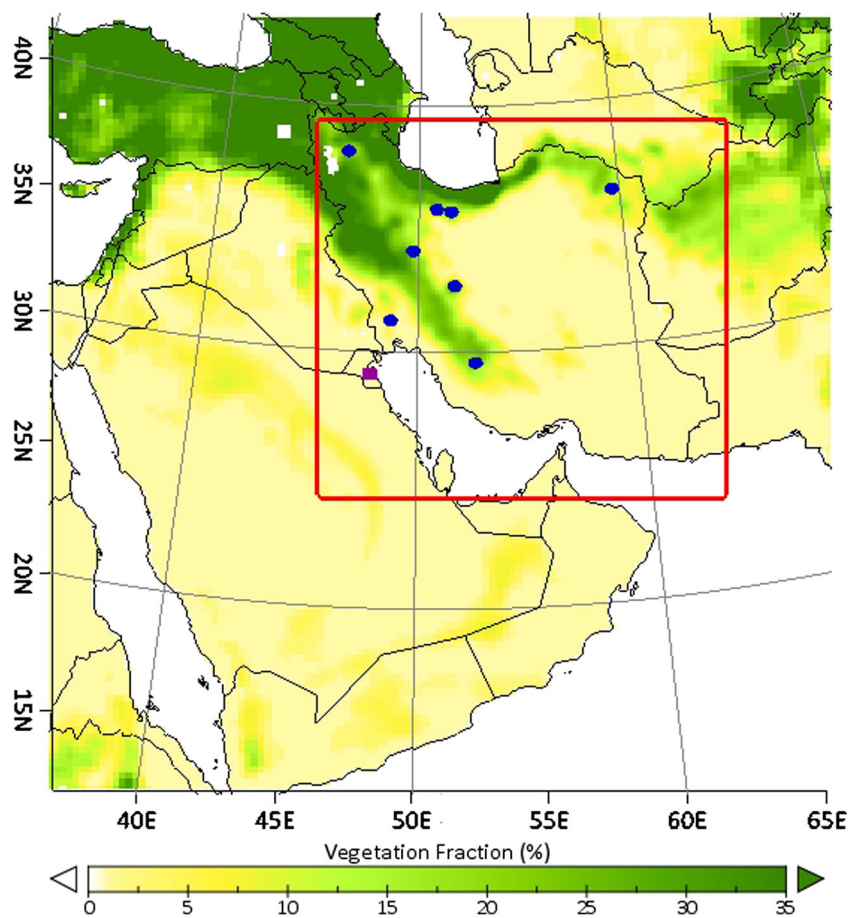
Model and data

WRF-Chem model

The weather research and forecasting model coupled with chemistry (WRF-Chem) is a state-of-the-art three-dimensional Eulerian chemical transport model. The dynamic solver core of the meteorology model (WRF) is based on fully compressible non-hydrostatic (also with a run-time hydrostatic option) Euler equations (Skamarock et al. 2008). The model consists of five main categories for physics options: microphysics, cumulus parameterization, planetary boundary layer, land surface model, and radiation. The fully online coupled chemistry component of the model uses same schemes and options used in meteorological component such as transport and physics schemes, time steps, and grids. The chemistry section of the model is composed of various schemes such as transport of chemical species, gas-phase and aerosol chemistry, aerosol-radiation feedback, aerosol emission and deposition, and photolysis frequencies (Grell et al. 2005).

For the present investigation, version 3.7.1 of WRF-Chem has been used in order to simulate dust emission and distribution, and also optical properties and radiative effects of mineral dust aerosols in the atmosphere during dust storms. As shown in Fig. 1, two domains are considered; the main domain covers most parts of the Middle East region (approximately latitude of 12° to 43° N , and longitude of 33° to 68° E) including Saudi Arabia, Iraq, Syria, Iran, Turkmenistan, and some parts of Afghanistan, Pakistan, and Turkey. The main domain consists of 120×120 horizontal grids with a spatial resolution of 30 km, and temporal resolution of 180 s. The nested domain is used in order to provide more focus and details over Iran. This domain covers Iran as well as some parts of neighboring countries such as Iraq, Saudi Arabia, Pakistan, and Turkmenistan (approximately latitude of 24° to 39° N , and longitude of 45° to 64° E). For this domain, the number of grids increased to 192×180 with the horizontal resolution of 10 km and temporal resolution of 60 s. It should be noted that in this article, any results over Iran refer to the nested domain which also includes some regions outside of

Fig. 1 Model domain shows vegetation fraction (%). *Red rectangle* indicates the nested domain. *Blue circles* show location of cities with air quality stations' data and *purple square* shows location of AERONET station used in this study



Iranian boundaries, except where otherwise stated. There are 30 vertical layers for both domains which continue to atmospheric pressure of 50 hPa (about 20 km) from the surface. Resolution of vertical layers varies from about 60 m near the surface to about 850 m for the top layer.

Considering the different properties of various schemes and results of the similar studies (e.g., Kumar et al. 2014), Purdue Lin microphysics scheme for water vapor and precipitation processes (Lin et al. 1983), Rapid Radiative Transport Model (RRTM) for both short-wave and long-wave radiation transfer (Mlawer et al. 1997), and Grell-3D scheme for parameterizing of sub-grid effects of convective and shallow clouds (Grell and Dévényi 2002) have been used. Also, MM5 similarity theory (Paulson 1970) for surface layer scheme has been selected, in which parameters like friction velocities and exchange coefficients are calculated. Moisture and heat fluxes have been provided using NOAA land surface model (Chen and Dudhia 2001) and also results from surface layer scheme. Furthermore, planetary boundary layer processes parameterization has been done by Yonsei University scheme (YSU) (Hong et al. 2006).

The second generation of Regional Acid Deposition Model (RADM2) (Stockwell et al. 1990) has been used for gas-phase chemical mechanism. This model includes 14 stable species, 4

reactive intermediates, and 3 abundant species (oxygen, nitrogen, and water) of inorganic chemicals, and also 26 stable species and 16 peroxy radicals of organic chemicals (Grell et al. 2005). For this study, processes of different types of aerosols (e.g., sulfate, black carbon, organic carbon, dust, and sea salt) have been calculated by Goddard Chemistry Aerosol Radiation and Transport (GOCART) (Ginoux et al. 2001; Chin et al. 2002). In addition, the inputs for the emission of anthropogenic pollutants including nitrogen oxides, greenhouse gases, volatile organic compounds (VOCs), and other species have been provided by using the REanalysis of the TROpospheric chemical composition (RETRO) (Schultz et al. 2007), as well as the Emission Database for Global Atmospheric Research (EDGAR) (Olivier et al. 1994) with a grid resolution of, respectively, 0.5° and 1.0°. Finally, the initial and lateral boundary conditions for meteorological fields were derived from Final Analysis (FNL) data, provided by National Center for Environmental Prediction (NCEP). The FNL data is available in 1.0° grid resolution and 6 h temporal resolution.

GOCART dust scheme (Ginoux et al. 2001) is used to calculate dust emission flux (F_p) by the following equation:

$$F_p = \begin{cases} CS_s(u_{10m})^2(u_{10m}-u_t), & u_{10m} > u_t \\ 0, & u_{10m} \leq u_t \end{cases} \quad (1)$$

where C is an empirical proportionality constant ($\mu\text{g}\cdot\text{s}^2\cdot\text{m}^{-5}$), S is the source function based on fraction of erodible soil, s_p represents the fraction of each size bin of dust, $u_{10\text{m}}$ is the horizontal wind speed at the altitude of 10 m, and u_t indicates threshold velocity for dust emission which is depended on particle size and surface moisture. The default value of C is $1 \mu\text{g}\cdot\text{s}^2\cdot\text{m}^{-5}$ (Ginoux et al. 2001). However, this constant is highly tunable for different conditions and regions to the extent that this value varies from 0.4 (Zhao et al. 2010; Kalenderski et al. 2013) to $22 \mu\text{g}\cdot\text{s}^2\cdot\text{m}^{-5}$ (Kumar et al. 2014) in different studies. For this study, the value of C initially has been tuned to $1.9 \mu\text{g}\cdot\text{s}^2\cdot\text{m}^{-5}$ which was proposed for using over Iran (Alizadeh-Chooari et al. 2014). Comparison between the estimated results and observational data obtained from Aerosol Robotic Network (AERONET) and air quality stations indicates an underestimate in both AOD and surface concentration. Therefore, the value of C has been increased to $4.0 \mu\text{g}\cdot\text{s}^2\cdot\text{m}^{-5}$ to achieve more accurate results.

Observational data

Three types of observational data have been used in this investigation for model configuration, determining dust storms and simulation period, and comparison with the model results. The first type is the data obtained from air quality monitoring stations in eight large cities throughout Iran (see Fig. 1). The other types of data are provided by AERONET (Holben et al. 2001). More than 600 globally distributed sites are used by AERONET for ground-based remote sensing of aerosol optical properties including AOD and single scattering albedo (SSA) in three quality levels. In addition, remote sensing data from different satellites have been used in the current work including Moderate Resolution Imaging Spectroradiometer (MODIS) and the Atmospheric Infrared Sounder (AIRS). MODIS is an instrument, designed and launched by NASA, aboard on Aqua and Terra satellites in order to improve scientific understanding of processes occurring on the land, and in the ocean and lower troposphere. AIRS is also a scanning instrument aboard on NASA's Aqua satellite for observing and characterizing atmospheric column for surface emissivity, profiles of temperature and humidity, and other atmospheric fields.

Using observational data for model configuration has been discussed in previous subsection. The comparison of model results and observations will also be discussed later in this article. In the following, the method used for identifying dust storms and simulation period are described. As mentioned earlier, the focus of the simulation is on Iran. Therefore, dust events with considerable both intensity and extensity have been searched for in order to evaluate the impacts of dust events all-over Iran. Mindful of the fact that PM_{10} concentration is a better indicator for dust aerosols' mass concentration, rather than $\text{PM}_{2.5}$ (Mahowald et al. 2014), the PM_{10}

concentrations, obtained from air quality monitoring stations, have been evaluated for eight large cities over Iran. This evaluation shows that in comparison with other cities higher concentration of PM_{10} is, usually, observed in Ahvaz. Thus, the days on which the PM_{10} concentrations were high (higher than $400 \mu\text{g}/\text{m}^3$ in Ahvaz and $200 \mu\text{g}/\text{m}^3$ in other cities) at least in three cities have been recorded. Nevertheless, depending only on monitoring stations' data could lead to greater uncertainties due to contribution of other types of aerosols, as well as lack of the stations' coverage for some parts of the country. Data obtained from AIRS have been used in order to increase the level of confidence in determining dust storms period. A product of AIRS which is called "Dust Score" has been used to evaluate the days with high dust concentrations. It should be noted that for some days and regions there were considerable differences between these two types of data. Finally, two dust storms (May 22–25, 2012 and April 22–25, 2015) have been identified as simulation periods by comparison of satellite and monitoring stations data. According to the results of the sensitivity analysis done by Zhang et al. (2015), a 48-h spin-up time is, also, considered before the simulation period.

Results and discussion

Dust emission rates

Using Eq. (1), dust emission rates are calculated for both domains. Figure 2 presents dust emission rates and wind vector fields at height of 10 m over the Middle East and Iran averaged over simulation periods. Strong winds, particularly northwesterly and westerly, over regions with low vegetation fraction (Fig. 1) and low altitudes (not pictured) bring about very high rates of dust emissions. Average wind speed (at height of 10 m) over the region which has been influenced predominantly by the Shamal winds (latitude of 21° to 37° N and longitude of 37° to 52° E) was 5.0 m/s during May-2012 dust event and 5.6 m/s during April-2015 dust event. However, the maximum wind speed in this region exceeds 18 m/s. For both dust storms, the sources with highest emission rates in the Middle East are Iraq alluvial plain, the Syrian Desert, the Arabian Desert (particularly Rub al-Khali and Ad-Dahna deserts), and the Karakum Desert in Turkmenistan. Nevertheless, for May-2012 dust event, central and southern arid regions of Oman were also among major emission sources. In addition to mentioned sources, the Makran Desert and Sistan Basin in Pakistan and Afghanistan also have a high dust emission rate. The most important emission source inside Iran is Khuzestan plain located in southwest of Iran (approximately 30 – 33° N and 48 – 50° E). There are also some other dust emission sources in Iran including Bushehr, Hormozgan, Sistan, and Baluchestan provinces in south and south east of Iran, Kavir and Lut Deserts, and

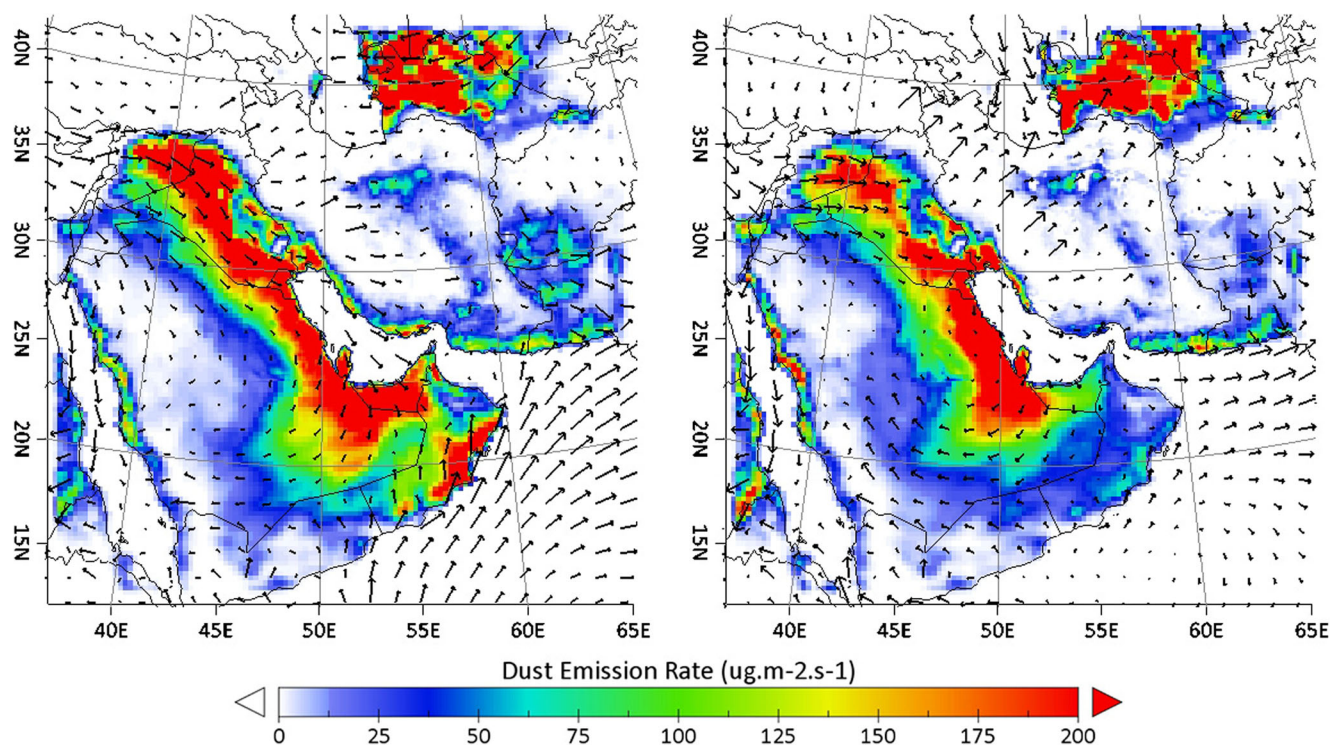


Fig. 2 Ten meter wind vector fields and spatial distribution of dust emission rates averaged over simulation period during May-2012 (*left*) and April-2015 (*right*) dust events

some provinces like Ilam located in west of Iran. The results show that 35 and 44 Tg dust emitted during May-2012 and April-2015 dust storms, respectively, over the nested domain. An approximate estimation from the results indicates that the contribution of emission sources inside Iran to total emission rate is about 7.1% for the first dust storm and about 8.0% for the second event.

As mentioned above, Khuzestan Province had much higher emission rate rather than other regions in Iran. The 24-h average emission rates for Khuzestan Province are respectively 154, 41, 62, and 64 $\mu\text{g}\cdot\text{m}^{-2}\cdot\text{s}^{-1}$ during May-2012 dust event and 123, 54, 152, and 109 $\mu\text{g}\cdot\text{m}^{-2}\cdot\text{s}^{-1}$ during April-2015 dust event.

Spatial distribution and impacts on air quality

The simulation results have been compared with different observational data which have been described in “[Observational data](#)” section. At the first step, MODIS (aboard Aqua) corrected reflectance (true color) images have been used in order to compare the spatial distribution of dust plume with the results of WRF-Chem simulation. Figure 3a shows a combination of four MODIS true color images over the simulation domain on 23 May 2012 between 09:05 to 10:50 AM. Since dust aerosols in all vertical levels are shown in MODIS images, these images have been compared with dust load (column concentration) simulated by WRF-Chem at 10:00 AM on

the same day (see Fig. 3b). Model results, similar to MODIS image, show a dense dust plume extended over southwestern to eastern parts of the Arabian Desert and high dust loads over northern coastal zones of the Persian Gulf. In MODIS image, also, dust aerosols can be detected over the Red Sea. However, model calculated high dust load over only a limited part of the Red Sea. Due to high cloud fraction on northern regions of the model domain, it is hard to compare model and MODIS image. Nevertheless, small visible part of the Caspian Sea indicates an overestimate of dust load by model for this region.

Similarly, a combination of multiple true color images captured by MODIS (Aqua) on April 25, 2015 between 08:45 to 10:30 AM (Fig. 3c) is compared with simulated dust load at 10:00 AM on the same day (Fig. 3d). The comparison shows that the model simulates dust load distribution correctly over the Arabian Desert, the Red Sea, and Turkmenistan.

Due to high wind speeds over regions with major dust emission sources (see Fig. 2), a considerable amount of dust particles is transported to the downstream regions. As shown in Fig. 4, May-2012 dust storm started by very high concentrations of dust over Iraq, coastal zones of the Persian Gulf, Oman, and some regions of Turkmenistan and the Caspian Sea on May 22. For instance, 24 h average surface dust concentration on this day exceeds $7500 \mu\text{g}/\text{m}^3$ over Balkan region in Turkmenistan. On the following day (May 23), dust plume extended to the south of Saudi Arabia and central regions of Iran. Simultaneously, dust emission of sources in southeast of Iran leads to high

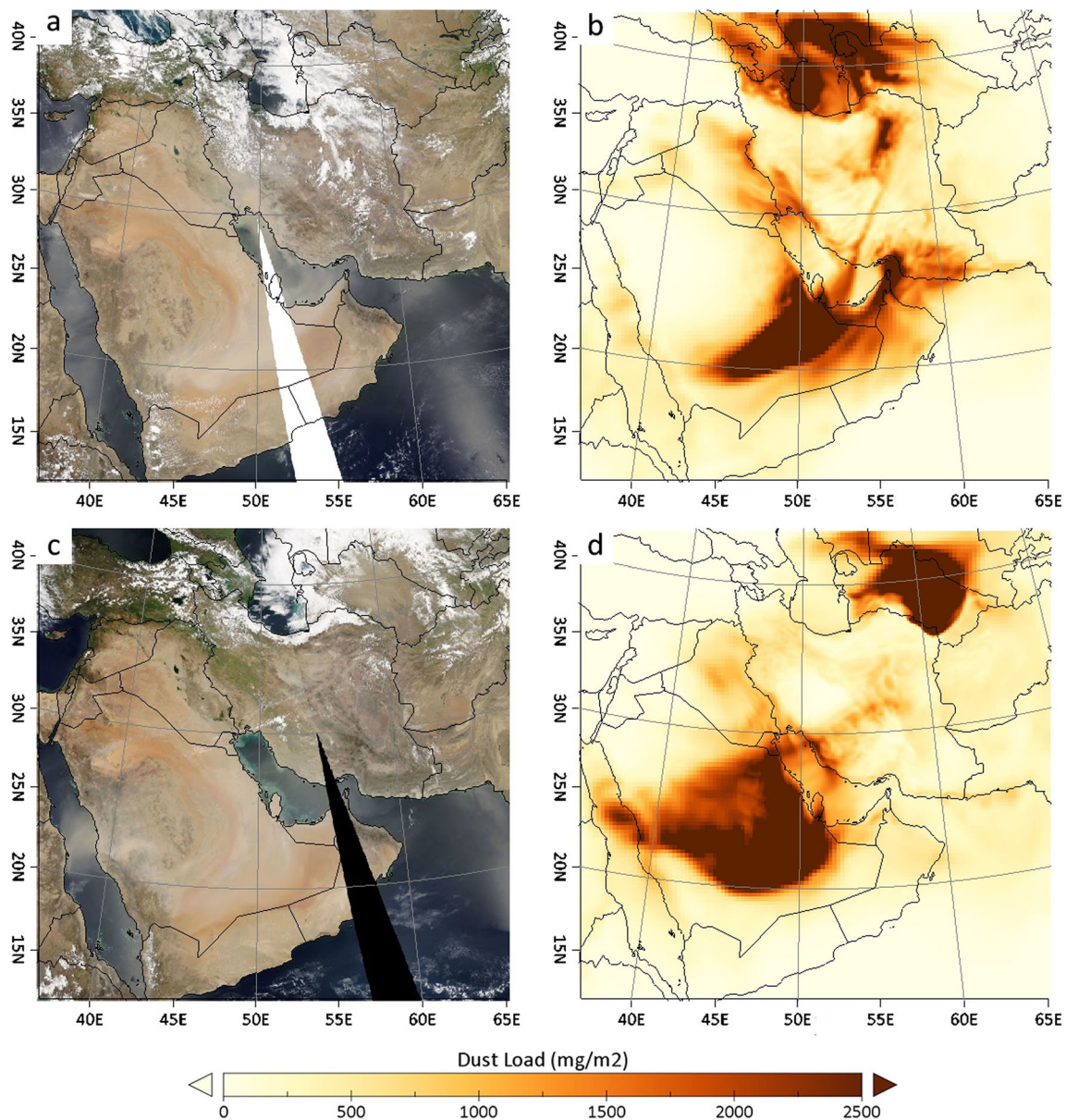


Fig. 3 Corrected reflectance image retrieved from MODIS at 09:00 to 10:50 on May 23, 2012 (a) and at 08:45 to 10:30 on April 25, 2015 (c). Dust load simulated by WRF-Chem at 10:00 on May 23, 2012 (b) and at 10:00 on April 25, 2015 (d)

concentration of dust over regions like Sistan and Baluchistan (border of Iran with Pakistan and Afghanistan). Decreasing trend of concentrations started on the third day (May 24), particularly for Iran and Turkmenistan. However, dust plume still remained over Iraq, south of Saudi Arabia, and some coastal regions of the Persian Gulf. Finally, on the last day of the dust event (May 25), high dust concentration restricted to only southeast of the Arabian Peninsula.

According to the results for April 2015 (see Fig. 5), dust storm started on April 22 when a dense dust plume formed over Iraq and some coastal zones of the Persian Gulf. On the second day of the dust event (April 23), there is not any major change in the spatial distribution of dust concentration, except

the slight increase over Turkmenistan and some parts of Iran, particularly western and central regions. A significant increase in dust concentration occurred on the third day (April 24) when most parts of Iraq, east of Saudi Arabia, and the Persian Gulf's coasts experienced very high dust loads. The dust plume on the last day of dust storm (April 25) not only has a great expansion, but also has an increase in concentration. On this day, most parts of Saudi Arabia (from the Red Sea to the Persian Gulf) and Turkmenistan affected by very high dust loads to the extent that 24 h average surface dust concentration reached $6200 \mu\text{g}/\text{m}^3$ over central part of Rub al-Khali Desert. In addition, Iraq, Oman, and central and south regions in Iran experience considerable dust concentration.

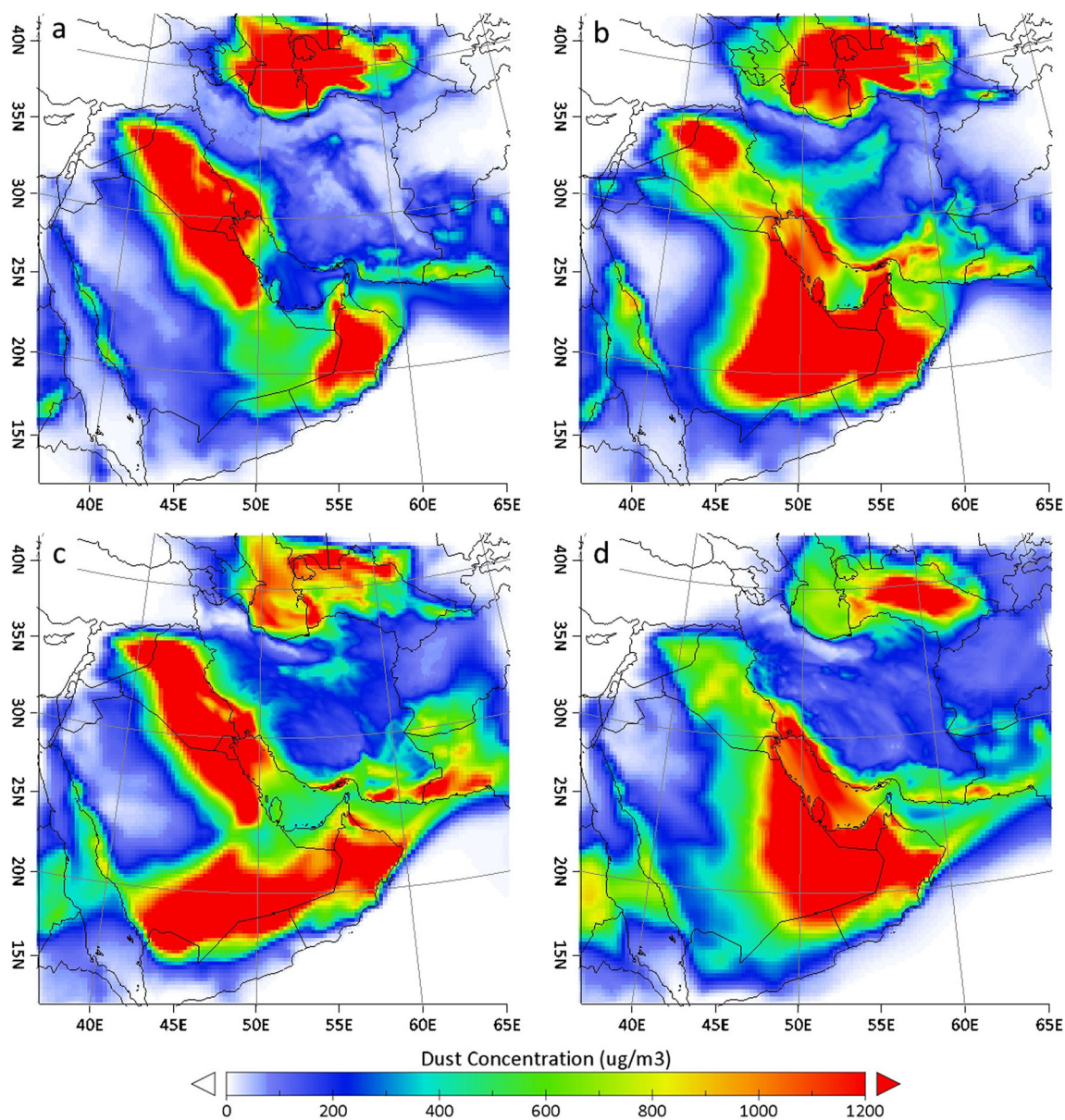


Fig. 4 Spatial distribution of 24-h average dust concentration on 22 (a), 23 (b), 24 (c), and 25 (d) May 2012

Figure 6 presents domain averaged dust mass concentration's vertical profile and time series for the nested domain (Iran). As it is shown, dust particles in May-2012 dust event ascended to higher altitudes (approximately 12 km) rather than April-2015 event (approximately 10 km). However, low concentrations (less than $75 \mu\text{g}/\text{m}^3$) are calculated above altitude of approximately 3 km and, also, dust concentrations above altitude of 6 km are almost negligible (less than $15 \mu\text{g}/\text{m}^3$).

Even though dust concentration in neighboring countries reaches higher values than Iran, simulated dust storms still have significant adverse impacts on air quality of cities throughout Iran. Surface dust concentration over Iran averaged over simulation period was $402 \mu\text{g}/\text{m}^3$ for May-2012 event, and $515 \mu\text{g}/\text{m}^3$ for April-2015 event. Considering the standard PM_{10} ambient concentration set by Iranian

Department of Environment ($150 \mu\text{g}/\text{m}^3$), dust concentrations exceed the standard limit in many cities in Iran, even without considering other types of particulate matters. Because of the proximity to major emission sources and lying on downstream direction, air quality in cities like Ahvaz and Shiraz affected by dust storms more severely rather than other cities. Particularly, high altitudes of the Zagros Mountains prevent dust plumes from reaching central regions of Iran. More details on dust concentration in different cities in Iran are summarized in Table 1.

Impacts on aerosol optical properties

The presence of dust particles in the atmosphere could affect the aerosol optical properties by absorbing and scattering of

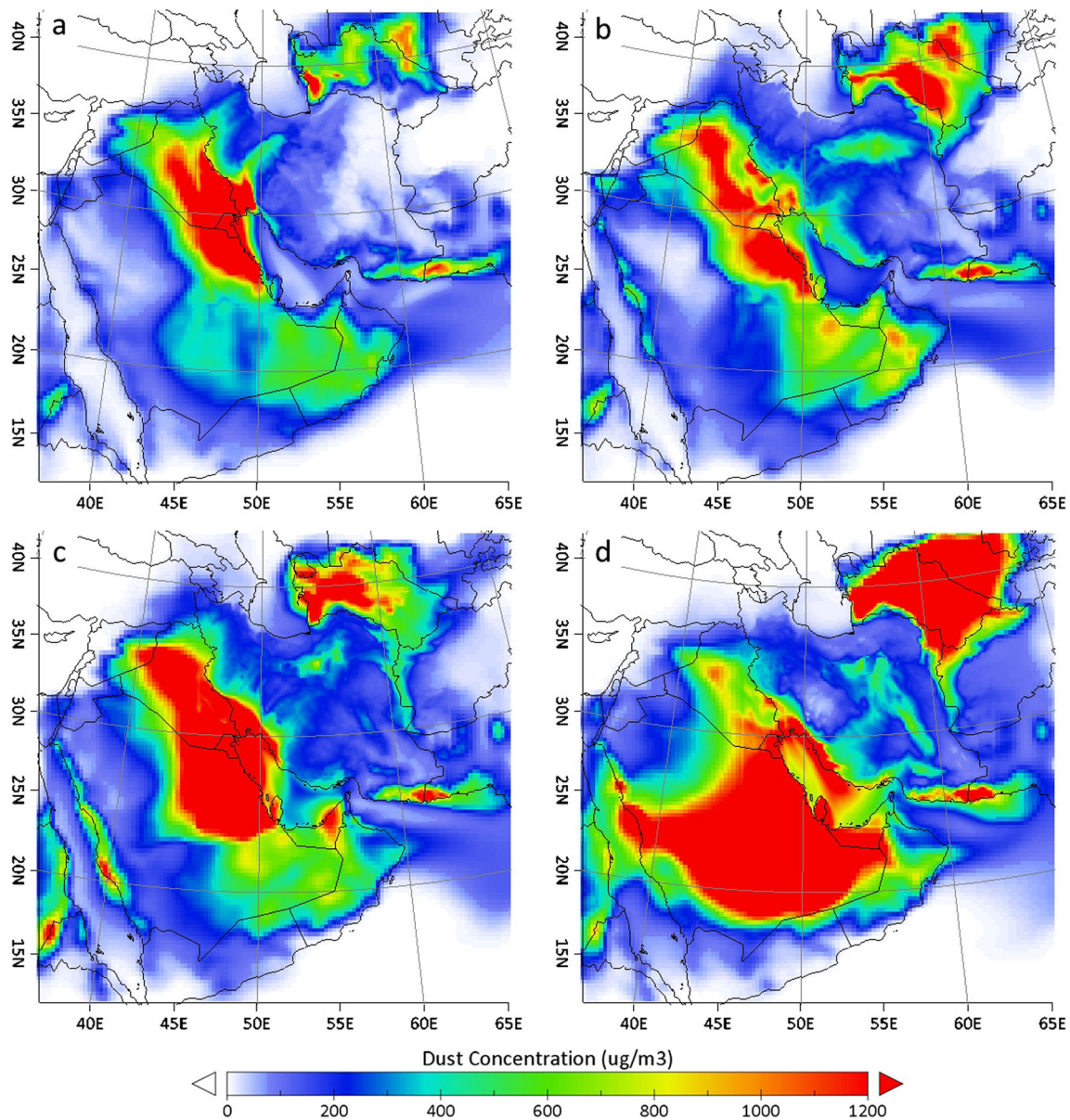


Fig. 5 Spatial distribution of 24-h average dust concentration on 22 (a), 23 (b), 24 (c), and 25 (d) April 2015

incident radiation. Several optical properties of aerosols such as SSA, extinction coefficient, and AOD are calculated by the schemes used in WRF-Chem model. In the following, results for the extinction coefficient and AOD are presented and discussed. Figure 7 shows the vertical profiles of extinction coefficient at 550 nm in three cities (Ahvaz, Shiraz, and Isfahan) in Iran at 05:00 on May 23, 2012 and April 23, 2015. As expected, extinction coefficient which is an indicator for the attenuation of radiation per unit of length has an inverse relation with the altitude, to the extent that extinction coefficient approaches to zero above 4 km altitude. The vertical profiles of extinction coefficient are very similar to profiles of dust concentration at the same time (not shown) which indicates insignificant effect of other types of particulate matters on optical properties during strong dust storms. However,

this might also be due to underestimation in the emission of other types of aerosols.

In addition to true color images, using the same date and time, AOD at 550 nm retrieved by MODIS (Aqua) has been compared with the simulation. Choosing combined Deep Blue and Dark Target AOD from MODIS products provides us to have more observation coverage over the simulation domain, particularly over bright surfaces such as deserts. However, there are still some parts of the domain which are not covered by MODIS observations. Also, impact of clouds on retrieving AOD (Feng et al. 2011) and limited temporal coverage of MODIS observations (twice a day) make the comparison restricted to a very few observations. The thick dust plume observed in Fig. 3a (on May 23, 2012) caused very high AOD extended from southern part of the Arabian Desert to central

Fig. 6 Vertical profile-time series of dust concentration averaged over Iran during May-2012 (*top*) and April-2015 (*bottom*) dust events

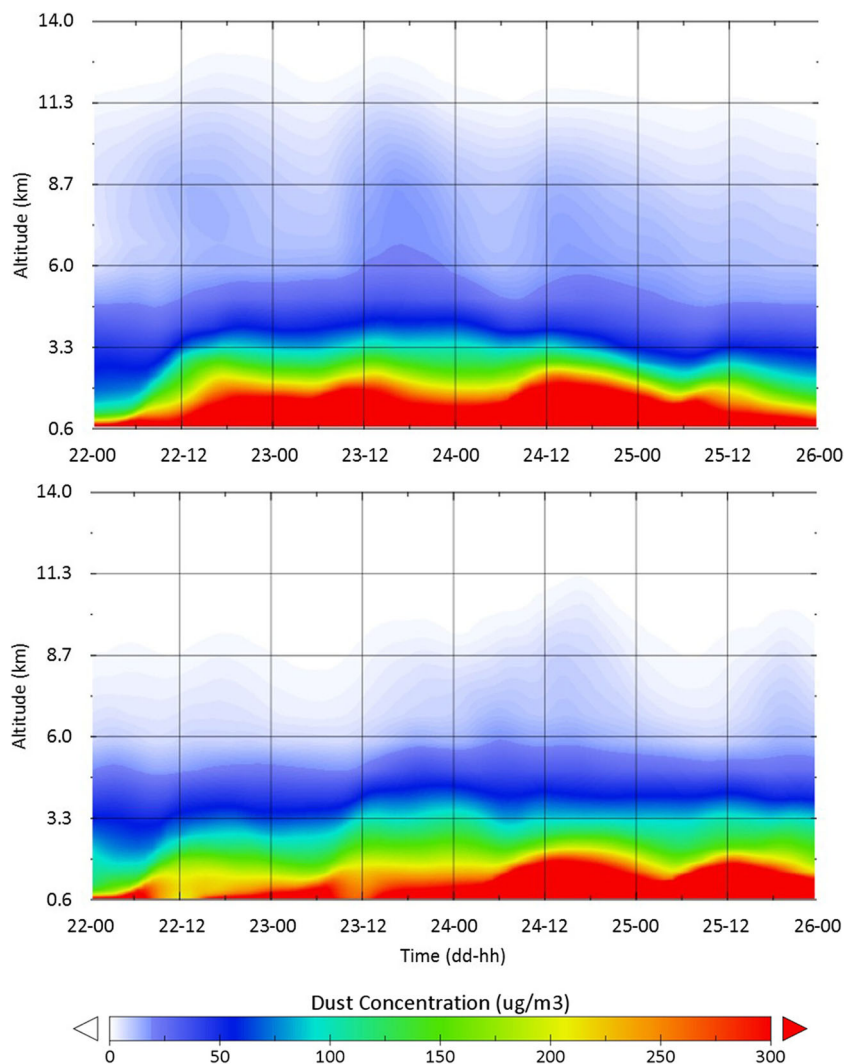


Table 1 Twenty-four-hour average surface dust concentration over several cities in Iran, simulated by WRF-Chem (all units are $\mu\text{g}/\text{m}^3$)

	May-2012				April-2015			
	22nd	23rd	24th	25th	22nd	23rd	24th	25th
Ahvaz (31.3N, 48.7E)	1613	824	1427	1164	2213	1084	1592	980
Isfahan (32.7N, 51.7E)	175	418	271	132	105	244	206	86
Mashhad (36.3N, 59.6E)	64	72	174	255	8	578	384	315
Shiraz (29.6N, 52.6E)	130	336	213	192	95	380	251	352
Tabriz (38.1N, 46.3E)	57	488	22	63	139	364	291	410
Tehran (35.7N, 51.4E)	51	59	110	53	159	126	176	166
Zahedan (29.5N, 60.9E)	50	269	301	147	33	51	186	129

parts of Iran (Fig. 8a). However, the model has calculated high AOD only at the Arabian Peninsula and smaller AOD is simulated over Iran (see Fig. 8b). Due to lack of data (white regions in Fig. 8a, c), comparison is not possible in some parts of the domain such as the Caspian Sea. As it is shown in Fig. 8c, d, there is an acceptable consistency between AOD retrieved by MODIS and simulated AOD by the model for April-2015 dust event. Nevertheless, limited available data show an overestimate of AOD in Turkmenistan. It should also be noted that a small dust plume visible in both MODIS images (see Figs. 3c and 8c) near 34° N, 52° E (west of the Kavir Desert) is not well simulated by WRF-Chem.

AERONET aerosol optical depth product has also been used in order to evaluate results of the model. Lack of stations with available/credible data during simulation period in Iran prompted the authors to use only stations outside Iran. However, there are still only few stations with available data outside Iran. Therefore, stations with level 1.5 data (automatically cloud cleared but not

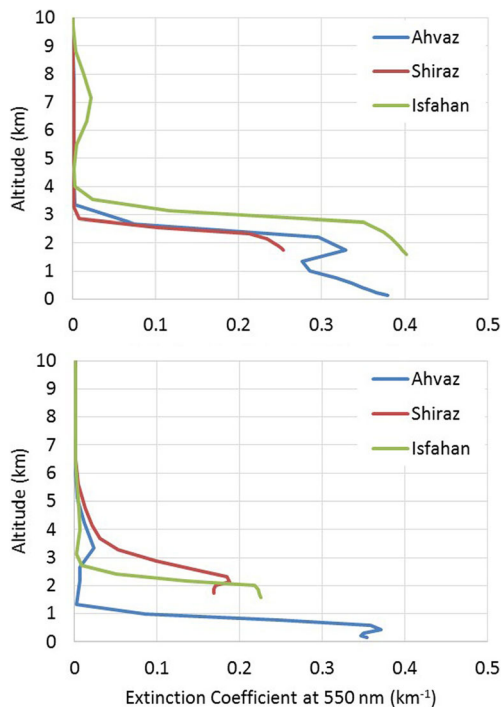


Fig. 7 Vertical profiles of extinction coefficient at 550 nm for cities of Ahvaz, Shiraz, and Isfahan at 5:00 on May 23, 2012 (*top*) and at 5:00 on April 23, 2015 (*bottom*) dust events

quality assured) have been considered in lieu of level 2 data (automatically cloud cleared, and pre- and post-field calibration applied). Finally, Kuwait University station (29.3° N, 48.0° E) has been chosen for the comparison (see Fig. 1). Result of the comparison is shown in Fig. 9. Totally, there are more underestimates during two simulated dust storms rather than few overestimates. One of the possible reasons for underestimated AOD by model would be the high uncertainties in anthropogenic aerosols emissions in southern and western Asia (Nair et al. 2012). Furthermore, paucity of quality-assured observation might also exacerbate the inconsistency between simulation results and observational data. Similar to the comparison with AOD retrieved by MODIS, evaluation of AERONET data indicates that the model simulated AOD during April-2015 more accurately than May-2012 dust storm.

Optical depth or thickness has been calculated by vertically integrating the extinction coefficient from ground surface to a given altitude. Optical depth (dimensionless) indicates the total attenuation of incident radiation between surface and a given altitude due to absorption and scattering by aerosols and gases. High dust concentrations during simulated dust storms significantly impact aerosol optical depth. As it is shown in Fig. 10, the high values of AOD are calculated where there are high concentrations of dust aerosols. For May-2012 dust storm, the AOD averaged over simulation period and domain is 0.26 in Middle East and 0.34 in Iran. However, 24 h averaged AOD reached much higher values in

regions under thick dust plume. For instance, average AOD on May 24 exceeds 2.4 in south of the Arabian Peninsula. It should also be noted that instantaneous AOD reached 4.0 in the same place. During April-2015, also, high values of aerosol optical depth are simulated. Time period and domain-averaged AOD over the Middle East and Iran are 0.19 and 0.30, respectively. Also, maximum 24 h average and instantaneous AOD have been simulated, both in the Karakum Desert in Turkmenistan, 1.9 and 3.9, respectively. The results indicate that AOD in neighboring arid regions of Iran has higher values rather than inside Iran. Nevertheless, regions with low dust concentrations in the Middle East such as Turkey and the Arabian Sea reduce the domain-averaged AOD in the Middle East.

Impacts on radiation budget

Two parallel simulations have been used in order to determine the impacts of dust particles on radiative flux at surface, top of atmosphere (TOA), and in the atmosphere. In the first simulation, all of the atmospheric pollutants have been considered, and the second simulation consists of all atmospheric pollutants except dust. Therefore, the difference between these two simulations shows the impact of dust aerosols on radiation budget.

Various terms are used to describe the impacts of aerosols on radiation. There are, however, some differences in their definitions. For instance, direct radiative effect (DRE) means instantaneous impact of aerosols on radiation, but direct radiative forcing (DRF) is the difference in DRE between pre-industrial and present day (Heald et al. 2014). Kumar et al. (2014) also proposed that radiation perturbation is more appropriate term in as much as the impacts of dust on radiation could also affect the distribution of clouds. As a result, radiative perturbation has been used in this investigation to describe the effects of dust aerosols on radiation. Radiative perturbation (F) is calculated using the following equation (McComiskey et al. 2008):

$$F = (f_a \downarrow - f_a \uparrow) - (f_0 \downarrow - f_0 \uparrow) \quad (2)$$

where f_a and f_0 denote radiative fluxes with and without presence of aerosols, respectively. Also, \downarrow indicates down welling flux and \uparrow indicates upwelling flux in Eq. (2).

In the presented work, daytime radiation perturbation (07:30 to 18:30 local time) for short-wave (SW), long-wave (LW), and net (SW + LW) radiations has been calculated and the results are illustrated in Figs. 11 and 12. For both case studies, high concentration of dust significantly affects radiation. The strongest radiative perturbations have occurred at the surface for SW radiation. This negative perturbation is largely due to attenuation of incoming radiation at the surface which

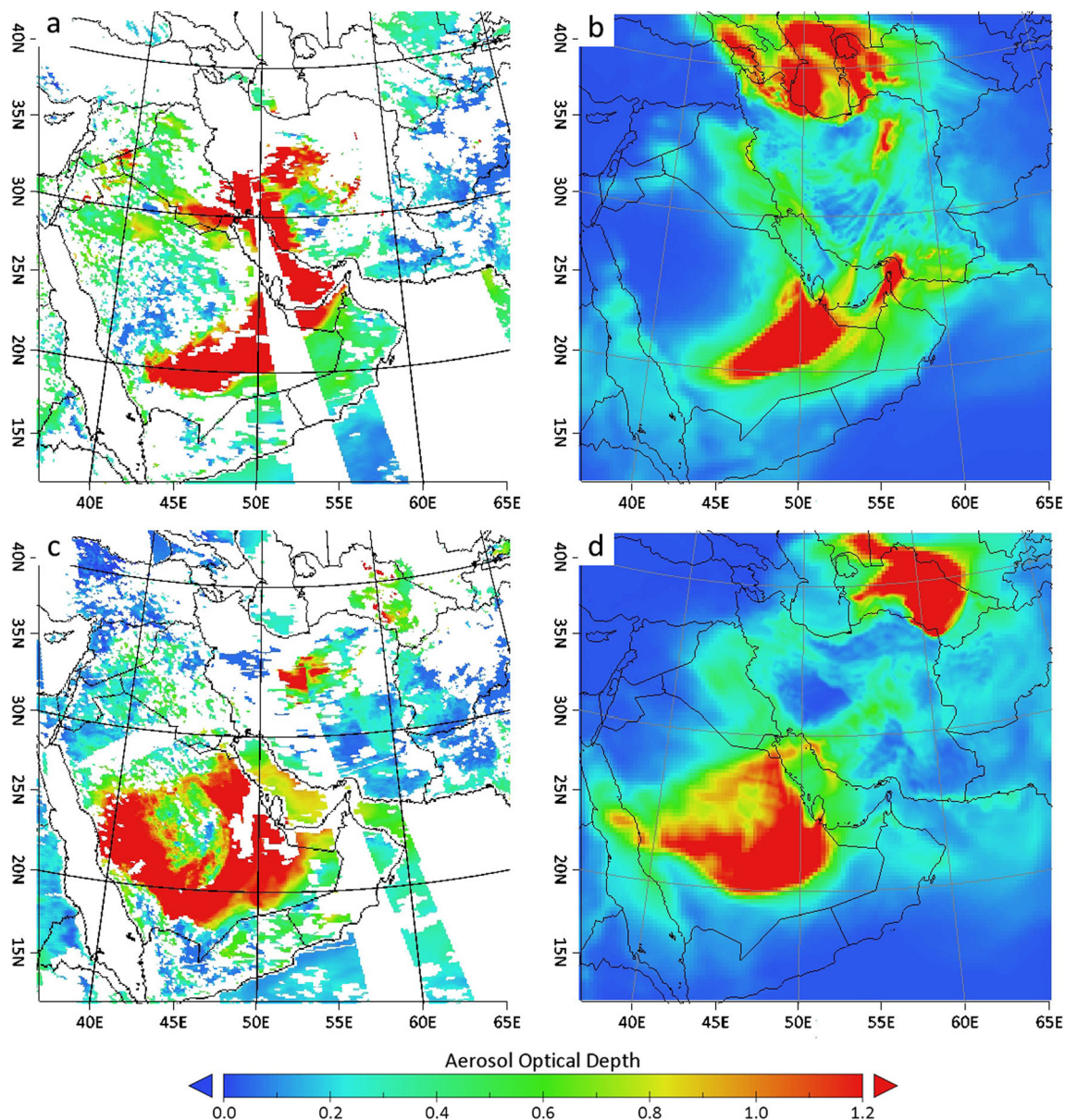


Fig. 8 AOD at 550 nm retrieved from MODIS at 09:00 to 10:50 on May 23, 2012 (a) and at 08:45 to 10:30 on April 25, 2015 (c). AOD at 550 nm simulated by WRF-Chem at 10:00 on May 23, 2012 (b) and at 10:00 on April 25, 2015 (d)

is caused by absorption and scattering of incident radiation by dust aerosols. During May-2012 and April-2015 dust storms, the average surface SW radiative perturbations in Iran were -24.2 and -21.7 W/m^2 , respectively. However, the maximum instantaneous perturbation is calculated to be -340 W/m^2 over the Caspian Sea, near the border of Iran and Azerbaijan, and -147 W/m^2 over the Persian Gulf for the two simulated dust storms. Also, simulation period and domain-averaged perturbation is estimated -18.8 and -13.5 W/m^2 over Middle East during May-2012 and April-2015 dust events, respectively.

In contrast with surface, SW radiative perturbations at TOA have moderate values and the negative and positive perturbations are almost balanced. It also has to be noted that surface albedo

affects TOA perturbation significantly, to the extent that TOA radiative perturbation is positive over bright surfaces such as deserts and negative over dark surfaces such as oceans. However, average perturbation at TOA is negative and much slighter than perturbation at surface (see Figs. 11 and 12). Domain and simulation period-averaged TOA radiative perturbations are estimated -0.31 and -3.6 W/m^2 over the Middle East and Iran, respectively, for May-2012 dust storm. Similarly, these values for April-2015 dust storm are simulated -0.37 and -3.9 W/m^2 over Middle East and Iran, respectively. Results for SW radiation in the atmosphere show strong positive radiative perturbation, since it is calculated by subtracting the surface from TOA perturbation. Average radiation perturbation in the

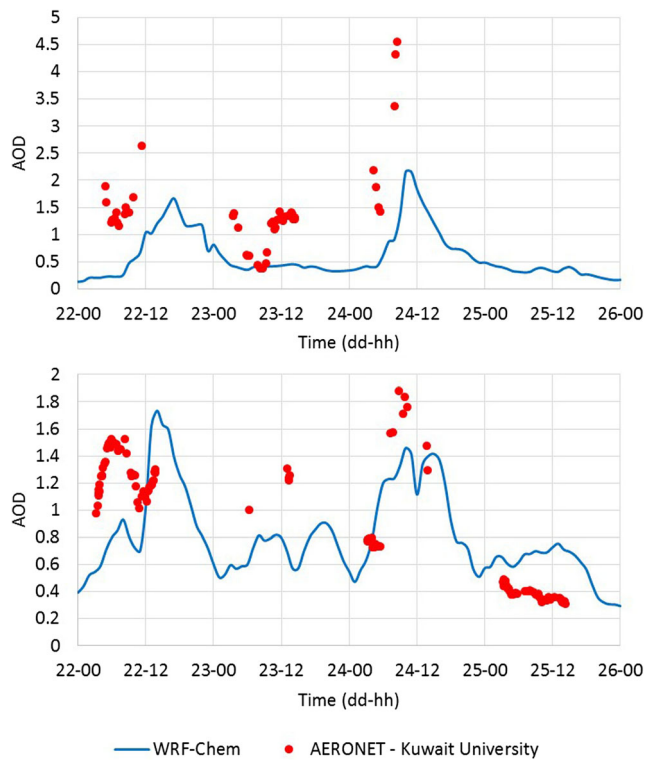


Fig. 9 AOD at 500 nm provided by Kuwait University AERONET station (red dots) and time series of AOD at 500 nm simulated by WRF-Chem (blue line) during May-2012 (top) and April-2015 (bottom) dust events

atmosphere over simulation period and domain are 20.6 and 17.8 W/m^2 over Iran, respectively, for May-2012 and April-2015 dust events.

Dust aerosols affect LW radiation in a different way. The downward long-wave re-emission of absorbed radiation and also trapping LW radiation from surface of the Earth by dust aerosols layer lead to a positive radiation perturbation at surface. At top of atmosphere, also, perturbation is positive but weak. As a result, calculated LW radiative perturbation in the atmosphere becomes negative. Nevertheless, LW perturbations, for all levels, are slighter than SW perturbation. Therefore, net radiative perturbation is more similar to SW perturbation. More details about the results of radiative perturbation are summarized in Table 2.

Impacts on meteorological parameters

The interaction between dust aerosols and radiation has also considerable effects on meteorological conditions. In this section, the impacts of dust storms on two meteorological fields, using parallel simulations, have been evaluated including surface sensible heat flux and surface temperature averaged over local daytime (07:30 to 18:30), nighttime (20:30 to 04:30), and 24 h separately.

As shown in Fig. 13, for both dust storms strong daytime negative heat flux perturbation is calculated due largely to absorption and scattering of incident light by dust particles. For instance, simulation period and domain-averaged perturbation of sensible heat flux are -5.4 and -5.0 W/m^2 over Iran for the first and second simulated dust events, respectively. However, maximum instantaneous heat flux perturbation over Iran reached -134 W/m^2 in May-2012 dust event and -110 W/m^2 in April-2015. It

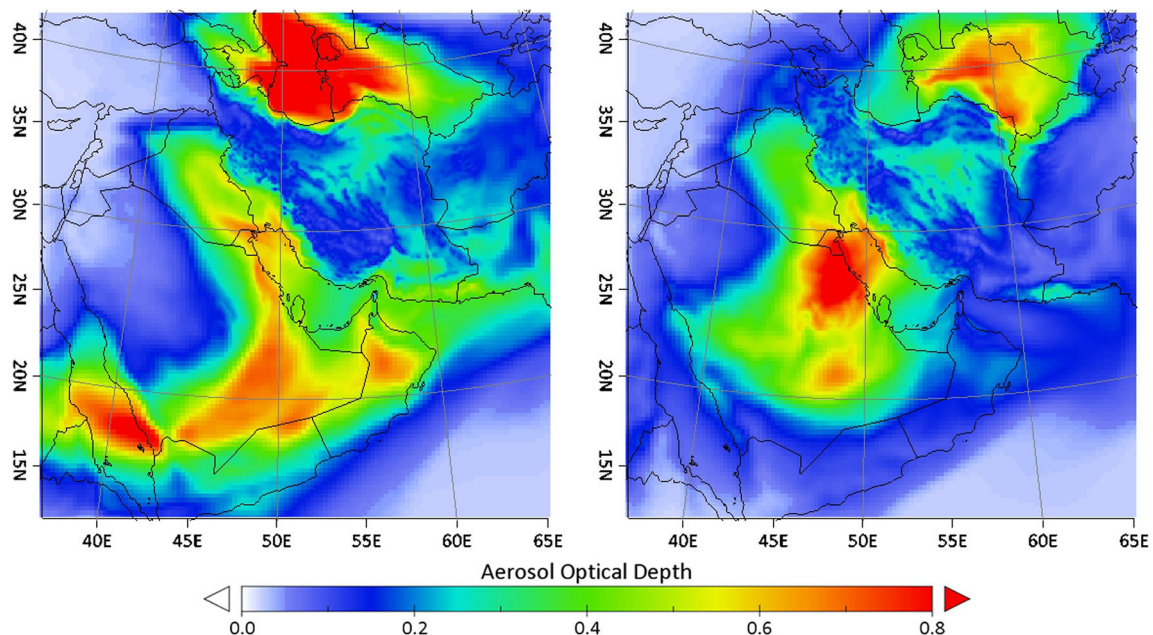


Fig. 10 Spatial distribution of average AOD at 550 nm during May-2012 (a) and April-2015 (b) dust events

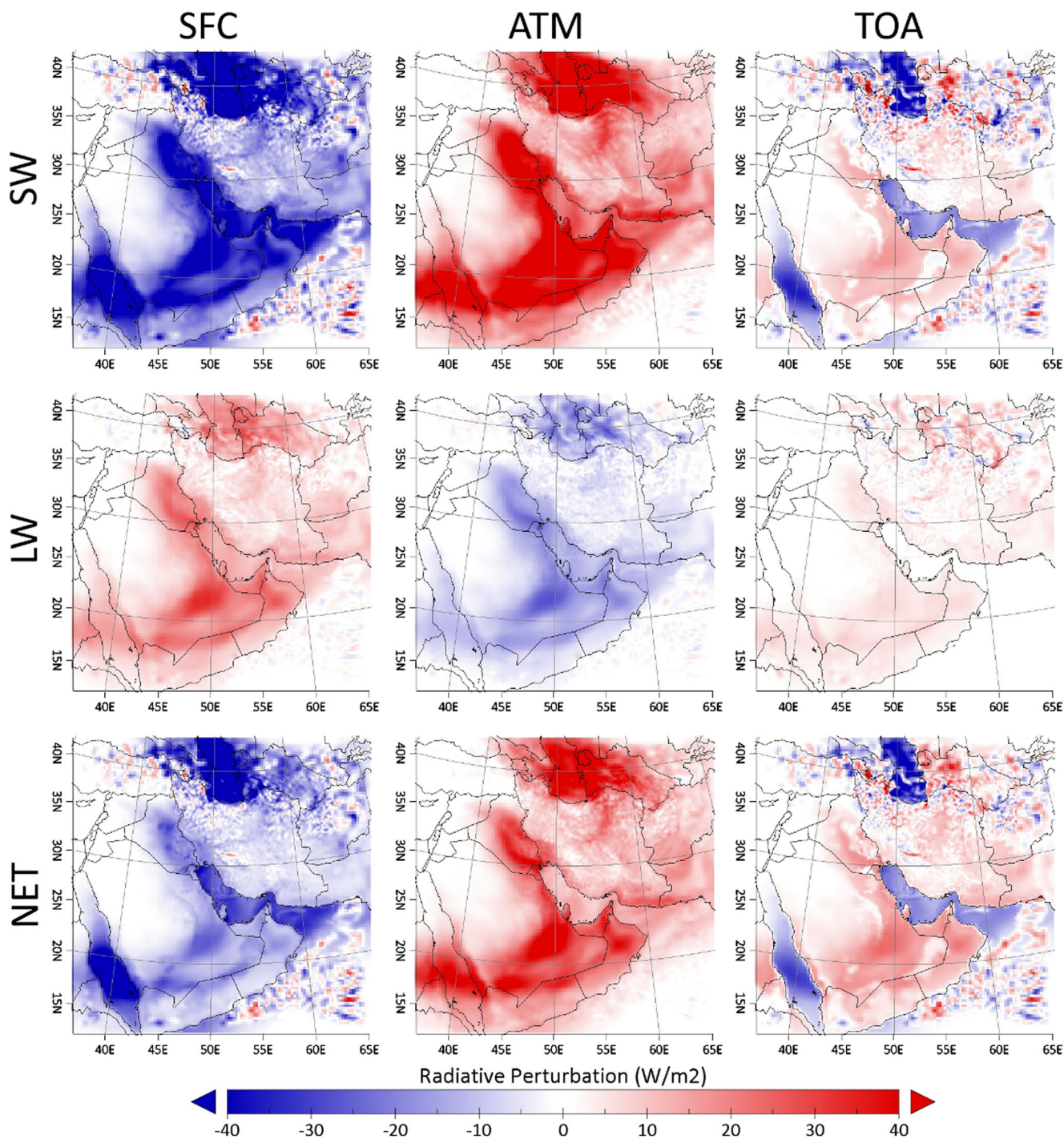


Fig. 11 Radiative perturbation of dust aerosols, averaged over simulation period for SW (top row), LW (middle row), and Net (bottom row) radiations at surface (left column), TOA (right column), and in the atmosphere (middle column) during May-2012 dust storm

has to be noted that in arid regions outside of Iran stronger perturbations are simulated. For example, instantaneous sensible heat flux exceeds $-162 W/m^2$ over the Karakum Desert in Turkmenistan. Nighttime positive dust-induced perturbations of heat flux are rather slighter than negative daytime perturbations, to the extent that average nighttime perturbations, for both dust storms, do not exceed $1.6 W/$

m^2 over Iran. As a result, 24 h average heat flux perturbation is negative in almost all of the domain, particularly in regions with high dust concentration, with average values of -2.3 and $-1.8 W/m^2$ during May-2012 and April-2015 dust events, respectively.

Similar to sensible heat flux, dust aerosols have a daytime cooling effect and nighttime warming effect on

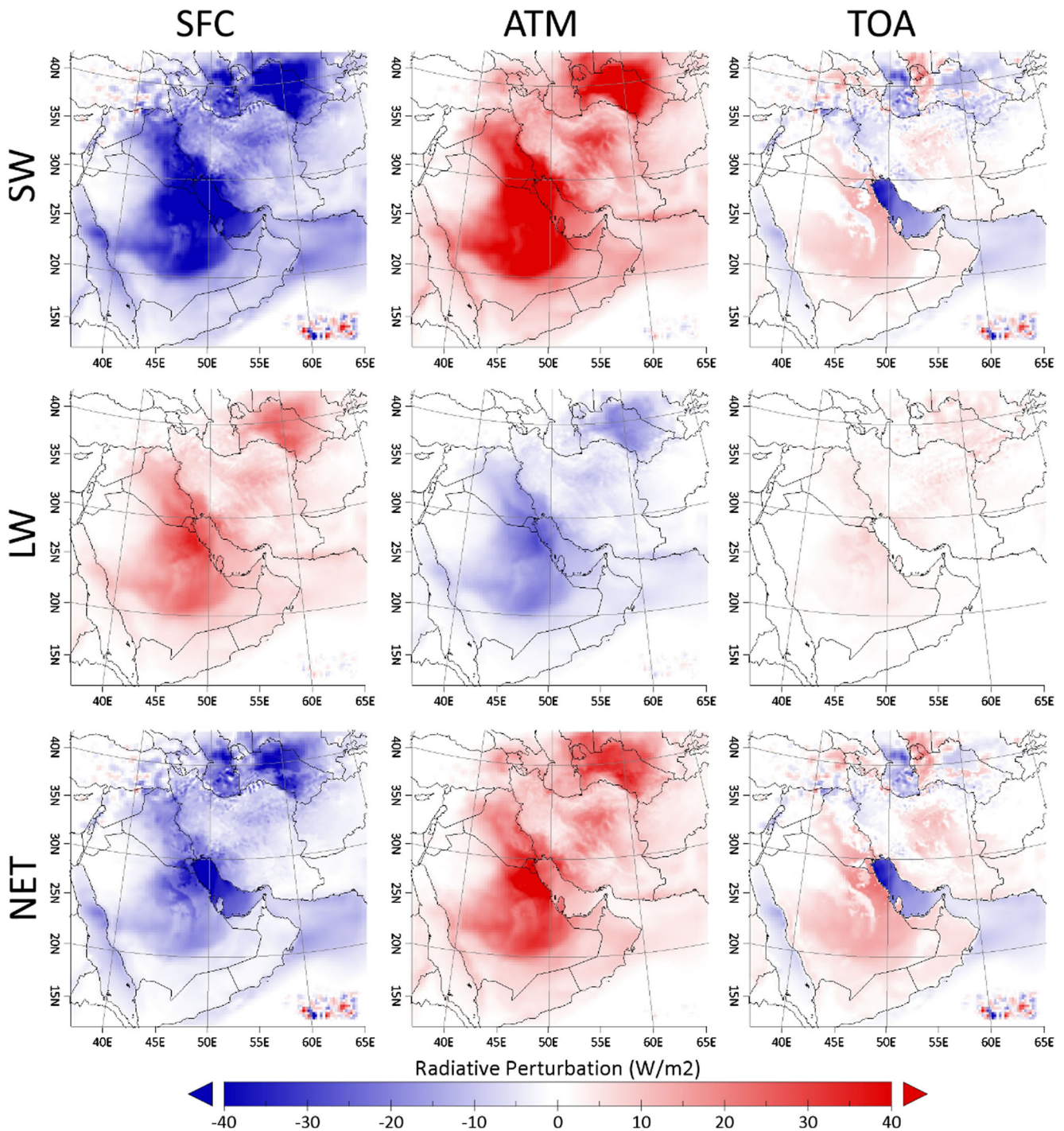


Fig. 12 Radiative perturbation of dust aerosols, averaged over simulation period for SW (top row), LW (middle row), and Net (bottom row) radiations at surface (left column), TOA (right column), and in the atmosphere (middle column) during April-2015 dust storm

surface temperature. Nevertheless, the main difference between these two parameters is that nighttime positive temperature perturbation is slightly stronger than negative daytime perturbation. Therefore, dust aerosols have a total warming effect on 24 h average surface temperature (see Fig. 14). Over Iran, simulation period and domain-

averaged daytime and nighttime temperature perturbations are -0.21 and 0.44 K during both simulated dust storms. However, much stronger instantaneous perturbations have occurred during both events. For instance, daytime temperature perturbation is calculated -13.4 K at 10:00 AM on May 23 2012 near border of Iran and

Table 2 Results of domain and simulation period averaged, and maximum instantaneous radiative perturbation over Iran

	May-2012						April-2015					
	SFC		ATM		TOA		SFC		ATM		TOA	
	Ave	Max	Ave	Max	Ave	Max	Ave	Max	Ave	Max	Ave	Max
SW	-24.2	-340	20.6	118	-3.6	-234	-21.7	-147	17.8	102	-3.9	-112
LW	9.7	69.0	-7.6	-53.8	2.1	77.2	9.6	55.9	-7.7	-48.0	1.9	37.5
Net	-14.5	-299	13.0	94.3	-1.5	-221	-12.1	-134	10.1	60.8	-2.0	109

Turkmenistan, and nighttime temperature perturbation exceeds 6.5 K near Riyadh City on April 25, 2015 at 01:00 AM.

Conclusions

WRF-Chem model has been used in this research work to simulate two strong dust storms (May 22–25, 2012 and

April 22–25, 2015) and their impacts on the Middle East with a focus on Iran. The dust storms have been identified using data provided by satellite remote sensing and air quality monitoring stations throughout Iran. Total dusts emitted from the nested domain are 35 and 44 Tg during May-2012 and April-2015 dust events, respectively. Iraq Alluvial plain, the Syrian Desert, Rub al-Khali and Ad-Dahna deserts in Saudi Arabia, and the Karakum Desert in Turkmenistan are identified as major dust emission sources. Also, in Iran, Khuzestan plain

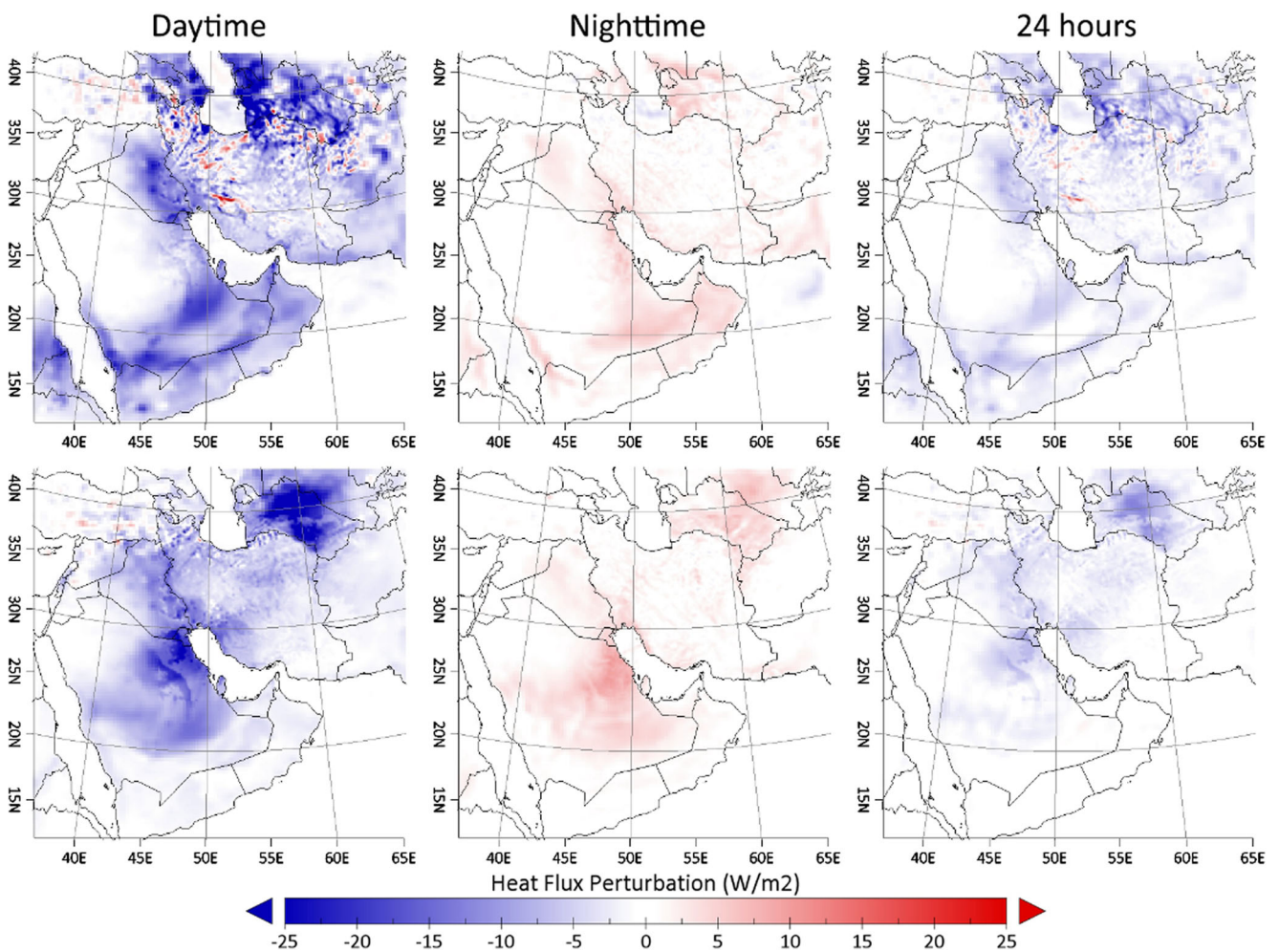


Fig. 13 Daytime (left column), nighttime (middle column), and 24 h (right column) sensible heat flux perturbation averaged over simulation period during May-2012 (upper row) and April-2015 (lower row) dust events

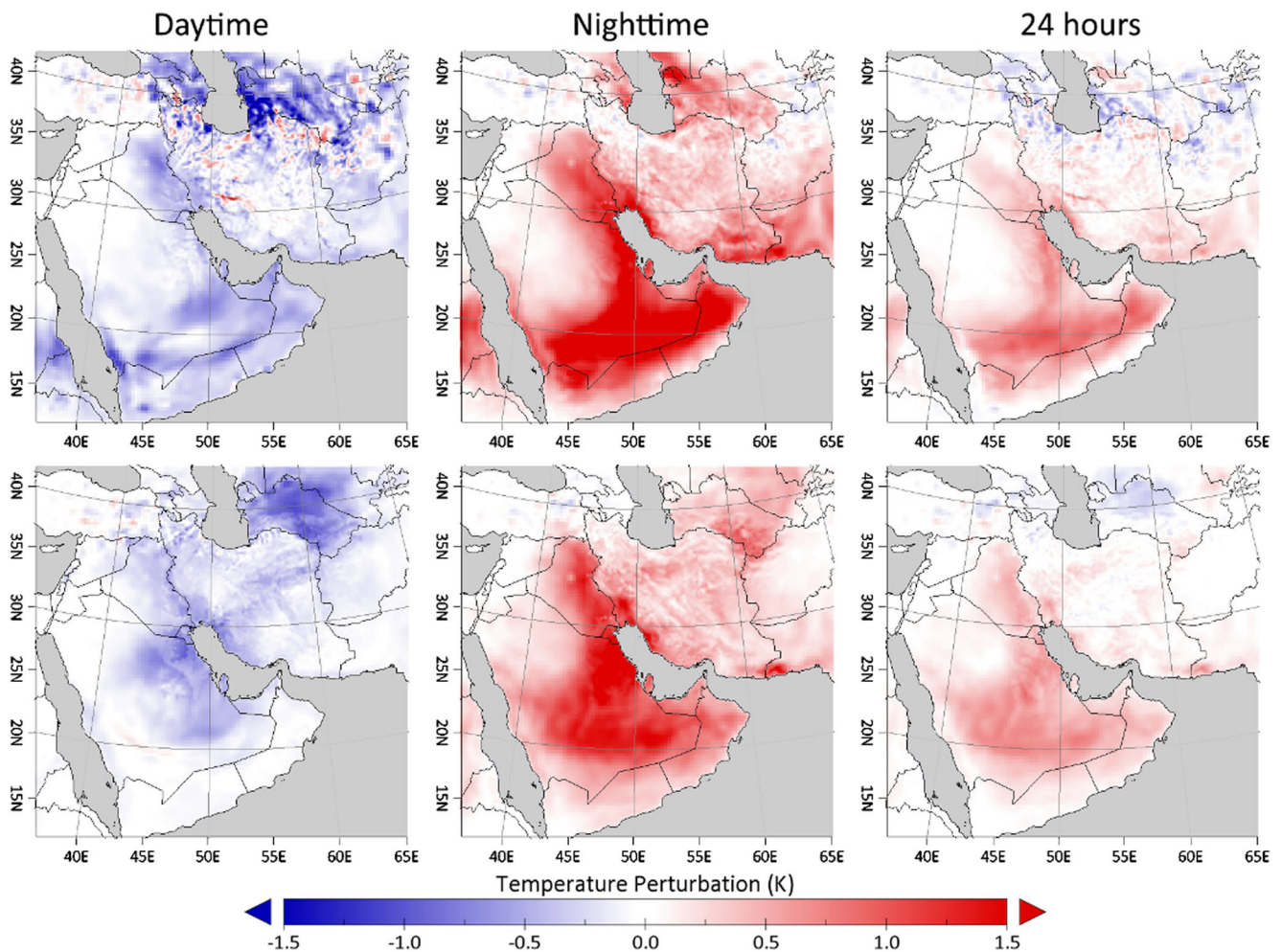


Fig. 14 Daytime (left column), nighttime (middle column), and 24 h (right column) surface temperature perturbation averaged over simulation period during May-2012 (upper row) and April-2015 (lower row) dust events

has much higher dust emission rates than the other sources. However, total emission in Iran is only a small fraction of total dust emitted in the Middle East. Two simulated dust storms had serious adverse impacts on air quality of cities throughout Iran, particularly cities like Ahvaz closest to the major dust emission sources. For instance, 24 h dust concentration exceeds $1600 \mu\text{g}/\text{m}^3$ on the first day of May-2012 dust event in Ahvaz. Nevertheless, complex topography such as high altitudes of the Zagros Mountains prevents dust plume from reaching cities in central regions of Iran such as Tehran. It has to be noted that dust concentrations had much higher values in neighboring countries and 24 h averaged values reached over $7000 \mu\text{g}/\text{m}^3$ in some regions like the Rub al-Khali and Karakum deserts. In addition, the results of the simulation have been compared with the observations. The comparison of the results with true color images retrieved by MODIS shows that the model could simulate dust spatial distribution over the domain.

The results of the simulation indicate the significant impacts of dust storms on aerosol optical properties. High values

of extinction coefficient have been calculated near the surface and, as expected, the values decrease at higher elevations. Also, AOD for both dust events reached very high values under the dust plume to the extent that instantaneous AOD is calculated 4.0 in the southern Arabian Peninsula. However, in comparison with AOD retrieved by MODIS, there is a general underestimate of AOD by the model, particularly for May-2012 dust event. High uncertainties of anthropogenic aerosols might be a reason for this underestimate. It has to be noted that AOD over Turkmenistan are overestimated for both dust storms. Consequently, presence of dust's high concentrations caused considerable impacts on radiation budget. The strongest radiative perturbations have occurred at surface and for SW radiation. The domain-averaged SW radiative perturbation during simulation period has been calculated -24.2 and $-21.7 \text{ W}/\text{m}^2$ at the surface over Iran, respectively, for May-2012 and April-2015 dust storms. Radiative perturbations at TOA are much slighter than perturbations at the surface and very dependent on surface albedo. There are also rather strong positive perturbations in the atmosphere. Since

weaker radiative perturbations have been calculated for LW radiation at all levels, distribution of net radiative perturbation is closer to SW perturbation rather than LW.

Simulated dust storms had also considerable effects on some meteorological fields. For both case studies, sensible heat flux at the surface has reduced in the daytime and increased in the nighttime. However, 24 h average heat flux perturbation is still negative. Results show that there is a negative diurnal temperature perturbation and a stronger positive nocturnal perturbation. As a result, 24 h average temperature perturbation has a warming effect.

Acknowledgments The authors thank Dr. Irannejad and Dr. Alizadeh-Choobari from Institute of Geophysics at the University of Tehran, and the anonymous reviewer for their helpful suggestions and comments on this article, and Dr. Niksokhan and Mr. Roozitalab from Computing Center at the Graduate Faculty of Environment for providing hardware facilities for this research work. We also acknowledge the principal investigators of AERONET station at Kuwait University for providing observational data. All MODIS and AIRS data products used in this investigation are obtained using EARTHDATA (<https://earthdata.nasa.gov>) and GIOVANNI (<http://giovanni.sci.gsfc.nasa.gov>). It should be noted that major parts of the visualization and analysis of the simulation's results have been done using Integrated Data Viewer (IDV) from UCAR/Unidata and Climate Data Operators (CDO). This research did not receive any specific grant from funding agencies from the public, commercial, or not-for-profit sectors.

References

- Alizadeh-Choobari O, Zawar-Reza P, Sturman A (2014) The “wind of 120days” and dust storm activity over the Sistan Basin. *Atmos Res* 143:328–341
- Alizadeh-Choobari O, Ghafarian P, Owlad E (2015) Temporal variations in the frequency and concentration of dust events over Iran based on surface observations. *Int J Climatol* 36:2050–2062
- Aryal R, Beecham S, Kamruzzaman M et al (2015) Temporal change of PM10 and its mass fraction during a dust storm in September 2009 in Australia. *Air Qual Atmos Health* 8:483–494
- Ashrafi K, Shafiepour-Motlagh M, Aslemand A, Ghader S (2014) Dust storm simulation over Iran using HYSPLIT. *J Environ Heal Sci Eng* 12:9
- Chen F, Dudhia J (2001) Coupling an advanced land surface—hydrology model with the Penn State—NCAR MM5 modeling system. Part I: model implementation and sensitivity. *Mon Weather Rev* 129:569–585
- Chen S, Huang J, Zhao C et al (2013) Modeling the transport and radiative forcing of Taklimakan dust over the Tibetan Plateau: a case study in the summer of 2006. *J Geophys Res Atmos* 118:797–812
- Chin M, Ginoux P, Kinne S et al (2002) Tropospheric aerosol optical thickness from the GOCART model and comparisons with satellite and Sun photometer measurements. *J Atmos Sci* 59:461–483
- Choobari OA, Zawar-Reza P, Sturman A (2014) The global distribution of mineral dust and its impacts on the climate system: a review. *Atmos Res* 138:152–165
- DeMott PJ, Prenni AJ, Liu X et al (2010) Predicting global atmospheric ice nuclei distributions and their impacts on climate. *Proc Natl Acad Sci* 107:11217–11222
- Feng Q, Hsu NC, Yang P, Tsay S-C (2011) Effect of thin cirrus clouds on dust optical depth retrievals from MODIS observations. *IEEE Trans Geosci Remote Sens* 49:2819–2827
- Giannadaki D, Pozzer A, Lelieveld J (2014) Modeled global effects of airborne desert dust on air quality and premature mortality. *Atmos Chem Phys* 14:957–968. doi:10.5194/acp-14-957-2014
- Ginoux P, Chin M, Tegen I et al (2001) Sources and distributions of dust aerosols simulated with the GOCART model. *J Geophys Res Atmos* 106:20255–20273
- Ginoux P, Prospero JM, Gill TE et al (2012) Global-scale attribution of anthropogenic and natural dust sources and their emission rates based on MODIS Deep Blue aerosol products. *Rev Geophys*. doi:10.1029/2012RG000388
- Grell GA, Dévényi D (2002) A generalized approach to parameterizing convection combining ensemble and data assimilation techniques. *Geophys Res Lett* 29:38-1–38-4
- Grell GA, Peckham SE, Schmitz R et al (2005) Fully coupled “online” chemistry within the WRF model. *Atmos Environ* 39:6957–6975
- Heald CL, Ridley DA, Kroll JH et al (2014) Contrasting the direct radiative effect and direct radiative forcing of aerosols. *Atmos Chem Phys* 14:5513–5527
- Holben BN, Tanre D, Smirnov A et al (2001) An emerging ground-based aerosol climatology: aerosol optical depth from AERONET. *J Geophys Res Atmos* 106:12067–12097
- Hong S-Y, Noh Y, Dudhia J (2006) A new vertical diffusion package with an explicit treatment of entrainment processes. *Mon Weather Rev* 134:2318–2341
- Huang X-X, Wang T-J, Jiang F et al (2013) Studies on a severe dust storm in East Asia and its impact on the air quality of Nanjing, China. *Aerosol Air Qual Res* 13:179–193
- Kakikawa M, Kobayashi F, Maki T et al (2008) Dustborne microorganisms in the atmosphere over an Asian dust source region, Dunhuang. *Air Qual Atmos Health* 1:195–202
- Kalenderski S, Stenchikov G, Zhao C (2013) Modeling a typical winter-time dust event over the Arabian Peninsula and the Red Sea. *Atmos Chem Phys* 13:1999
- Kumar P, Sokolik IN, Nenes A (2011) Measurements of cloud condensation nuclei activity and droplet activation kinetics of fresh unprocessed regional dust samples and minerals. *Atmos Chem Phys* 11:3527–3541
- Kumar R, Barth MC, Pfister GG et al (2014) WRF-Chem simulations of a typical pre-monsoon dust storm in northern India: influences on aerosol optical properties and radiation budget. *Atmos Chem Phys* 14:2431–2446
- Lin Y-L, Farley RD, Orville HD (1983) Bulk parameterization of the snow field in a cloud model. *J Clim Appl Meteorol* 22:1065–1092
- Liu L, Huang X, Ding A, Fu C (2016) Dust-induced radiative feedbacks in north China: a dust storm episode modeling study using WRF-Chem. *Atmos Environ* 129:43–54
- Mahowald NM, Kiehl LM (2003) Mineral aerosol and cloud interactions. *Geophys Res Lett*. doi:10.1029/2002GL016762
- Mahowald N, Albani S, Kok JF et al (2014) The size distribution of desert dust aerosols and its impact on the earth system. *Aeolian Res* 15:53–71. doi:10.1016/j.aeolia.2013.09.002
- McComiskey A, Schwartz SE, Schmid B et al (2008) Direct aerosol forcing: calculation from observables and sensitivities to inputs. *J Geophys Res Atmos*. doi:10.1029/2007JD009170
- Mlawer EJ, Taubman SJ, Brown PD et al (1997) Radiative transfer for inhomogeneous atmospheres: RRTM, a validated correlated-k model for the longwave. *J Geophys Res Atmos* 102:16663–16682
- Nair VS, Solmon F, Giorgi F et al (2012) Simulation of South Asian aerosols for regional climate studies. *J Geophys Res Atmos*. doi:10.1029/2011JD016711
- Olivier JGJ, Bouwman AF, der Maas CWM, Berdowski JJM (1994) Emission database for global atmospheric research (EDGAR). In: Non-CO₂ greenhouse gases: why and how to control? Springer, pp 93–106

- Paulson CA (1970) The mathematical representation of wind speed and temperature profiles in the unstable atmospheric surface layer. *J Appl Meteorol* 9:857–861
- Prospero JM, Ginoux P, Torres O et al (2002) Environmental characterization of global sources of atmospheric soil dust identified with the Nimbus 7 Total Ozone Mapping Spectrometer (TOMS) absorbing aerosol product. *Rev Geophys*. doi:10.1029/2000RG000095
- Rezazadeh M, Irannejad P, Shao Y (2013) Climatology of the Middle East dust events. *Aeolian Res* 10:103–109
- Satheesh SK, Krishna Moorthy K (2005) Radiative effects of natural aerosols: a review. *Atmos Environ* 39:2089–2110
- Schultz MG, Backman L, Balkanski Y, et al (2007) REanalysis of the TROpospheric chemical composition over the past 40 years (RETRO)—a long-term global modeling study of tropospheric chemistry. Final Report, Jülich/Hamburg, Ger 1–122
- Shahsavani A, Naddafi K, Haghhighifard NJ et al (2012) The evaluation of PM₁₀, PM_{2.5}, and PM₁ concentrations during the Middle Eastern Dust (MED) events in Ahvaz, Iran, from April through September 2010. *J Arid Environ* 77:72–83
- Shao Y (2008) Physics and modelling of wind erosion. Springer Science & Business Media
- Skamarock WC, Klemp JB, Dudhia J, et al (2008) A description of the advanced research WRF Version 3. Natl Cent Atmos Res Boulder Co Mesoscale Microscale Meteorol Div 1–113
- Stockwell WR, Middleton P, Chang JS, Tang X (1990) The second generation regional acid deposition model chemical mechanism for regional air quality modeling. *J Geophys Res Atmos* 95:16343–16367
- Zhang Y, Liu Y, Kucera PA et al (2015) Dust modeling over Saudi Arabia using WRF-Chem: March 2009 severe dust case. *Atmos Environ* 119:118–130
- Zhao C, Liu X, Leung LR et al (2010) The spatial distribution of mineral dust and its shortwave radiative forcing over North Africa: modeling sensitivities to dust emissions and aerosol size treatments. *Atmos Chem Phys* 10:8821–8838
- Zhao C, Liu X, Ruby Leung L, Hagos S (2011) Radiative impact of mineral dust on monsoon precipitation variability over West Africa. *Atmos Chem Phys* 11:1879–1893